www.springer.com/41230
https://doi.org/10.1007/s41230-022-1109-z

Morphologies of intermetallic compound phases in Sn-Cu and Sn-Co peritectic alloys during directional solidification

***Peng Peng[1, 2, 3], Jin-mian Yue[4], An-qiao Zhang[1], Jia-tai Wang[3], and Jiang-lei Fan[5]**

1. School of Physics and Electronic Information Engineering, Qinghai Normal University, Xining 753000, China

2. School of Materials and Energy, Lanzhou University, Lanzhou 730000, China

3. Northwest Rare Metal Materials Research Institute, Shizuishan 753099, Ningxia, China

4. Shanxi Taigang Stainless Steel Co., Ltd., Taiyuan 030003, China

5. School of Mechanical and Electrical Engineering, Zhengzhou University of Light Industry, Zhengzhou 450000, China

Abstract: The morphologies of intermetallic phases (IMCs) during directional solidification of the Sn-Cu ($L+Cu_3Sn \rightarrow Cu_6Sn_5$) and Sn-Co ($L+CoSn \rightarrow CoSn_2$) peritectic systems were analyzed. The primary Cu_3Sn and peritectic Cu_6Sn_5 phases in Sn-Cu alloy are IMCs whose solubility ranges are narrow, while both the primary CoSn and peritectic $CoSn_2$ phases in Sn-Co alloy are IMCs whose solubility ranges are nil in equilibrium condition. The experimental results before acid corrosion shows that the dendritic morphology of both the Cu_6Sn_5 and $CoSn_2$ phases can be observed. The investigation on the local dendritic morphology after deep acid corrosion shows that these dendrites are composed of small sub-structures with faceted feature. Faceted growth of the primary Cu_3Sn and CoSn phases is also confirmed, and a faceted to non-faceted transition in their morphologies is observed with increasing growth velocities. Further analysis shows that the dendritic morphology is formed in the solidified phases whose solubility range is larger during peritectic solidification.

Keywords: intermetallic compound phase; peritectic alloy; directional solidification; solubility range; sub-structure

CLC numbers: TG146.1+4 **Document code:** A **Article ID:** 1672-6421(2022)05-411-08

1 Introduction

Numerous research works have been performed for peritectic alloys which can be used in broad industrial applications [1-6]. The peritectic reaction: $L+\alpha \rightarrow \beta$ occurs during solidification of these systems, where α is the primary phase and β is the peritectic phase [7]. Three different types of peritectic systems can be defined depending on whether the solid phases involved are solid solution phases or intermetallic compound phases (IMCs) with nil solubility or narrow solubility range [7]. Different from the solid solution phases which have been commonly analyzed, the growth of IMCs from melt is of practical interest because the appropriate morphology, size, and distribution of IMCs can lead to significant optimizing properties of alloys [8-13]. Furthermore, IMCs exhibit more complex morphologies as compared with the solid solution phases: planar, cellular to dendritic [14]. Faceted growth with a strong anisotropy can often be observed during solidification of IMCs. In addition, the transition from faceted growth to nonfaceted growth with increasing cooling rates have also been confirmed [15, 16].

However, the current analyses on the morphology of solidification microstructure are usually based on two-dimensional observation [17, 18], which is limited since the three-dimensional information of the growth morphology can not be fully revealed [19]. In recent decades, many methods have been developed to characterize the three-dimensional morphology of solid phases. Three of these methods have been most widely used: three-dimensional reconstruction on the basis of three-dimensional successive sectioning [20, 21], synchrotron radiation [22], and the deep etching method using appropriate acid/alkali corrosion. Among them, the deep etching method has shown strong applicability, and its only difficulty lies in choosing an appropriate corrosive to better exhibit the morphology information. For this reason, the morphology information of many phases [8-13] including both solid solution phase and IMCs have been obtained through the deep etching method.

***Peng Peng**

Ph. D., Professor. His research interests mainly focus on the solidification theory of nonferrous alloys (Sn-base, and TiAl alloys) during directional solidification, and advanced casting processes of structural superalloys (Ni-base alloys).

E-mail: pengp@lzu.edu.cn

Received: 2021-08-28; Accepted: 2022-04-29

The IMCs can be frequently encountered in solidification of different peritectic systems. Among them, the Sn-Cu and Sn-Co alloys have shown wide application. As one of the most popular lead-free solders, Sn-Cu alloys are commonly applied in the electronics industry owing to their excellent weldability and non-toxic property [23-29]. Investigation on the Sn-Cu solders of high Sn content is of great interest since the operating temperature of solders can be enhanced by increasing the content of Cu. Sn-Co alloys are also widely used in lead-free solders, negative electrode materials, etc [30-35]. In Sn-based solders used in electronic packaging, Co can form a good diffusion barrier between solder and substrate due to its low solubility [36-38].

Despite the numerous reports on Sn-Cu and Sn-Co peritectic systems, the study on the three-dimensional morphology of these peritectic systems containing IMCs has been rarely reported. Further experimental evidences are required for understanding the growth of the IMCs in detail in these peritectic alloys. In this work, the morphology features of IMCs were analyzed in the Sn-Cu and Sn-Co peritectic alloys through deep etching method. Furthermore, the dependence of the formation of dendritic morphology on the solubility range of the solidified phases was also investigated.

2 Experimental procedure

Pure copper (99.9wt.%), pure tin (99.9wt.%) and cobalt (99.9wt.%) were used as raw materials to prepare the Sn-32at.% Cu and Sn-9at.% Co alloys by melting in a vacuum induction furnace. The rods (Φ6 mm×80 mm) were cut from the ingot and placed into the Al_2O_3 tubes [φ6.5(Φ7.5) mm×110 mm]. Directional solidification was carried out in a Bridgman-type apparatus. First, the furnace was heated up above their melting temperature (600 ºC for Sn-Cu and 850 ºC for Sn-Co), and held for 30 min. Second, the Sn-32at.% Cu and Sn-9at.% Co samples were fabricated at different growth velocities: 10, 20 μm·s^{-1} for Sn-32at.% Cu alloy and 1, 5, 10, 100 μm·s^{-1} for Sn-9at.% Co alloy. After that, the tube was quickly quenched into the liquid Ga-In-Sn alloy. The temperature gradient during directional solidification of both alloys is 32 K·mm^{-1}, which was obtained from the temperature profiles of the PtRh30-PtRh6 thermocouples near the solid/liquid interface. Finally, the microstructures on the longitudinal sections of the samples were analyzed using scanning electron microscopy (SEM, Apreo-S) equipped with energy dispersive spectrometer (EDS). An etchant solution of 10 g $FeCl_3$+40 mL HCl+160 mL C_2H_5OH was used to dissolve the eutectic matrix and preserve the 3D morphologies of the IMCs.

3 Results

According to phase diagrams shown in Fig. 1, the Sn-32at.% Cu alloy experiences the solidification of the primary Cu_3Sn phase at 530 ºC [23, 26, 27]: L→Cu_3Sn, then the peritectic reaction at T_P=415 ºC: L+Cu_3Sn→Cu_6Sn_5, and the eutectic reaction at T_E=231.96 ºC. The Sn-9at.% Co alloy experiences the solidification of the primary CoSn phase at 810 ºC: L→CoSn, the peritectic reaction at T_P=525 ºC [31-33]: L+CoSn→$CoSn_2$, and eutectic reaction at T_E=231.96 ºC.

The microstructures of the directionally solidified Sn-32at.% Cu peritectic alloys before deep etching are given in Fig. 2. The dark gray (25.7at.% Sn) and light gray (43.7at.% Sn) phases are determined to be the Cu_3Sn, Cu_6Sn_5 phases through the EDS analysis. As can be seen in Fig. 2, the primary ε-Cu_3Sn phase exhibits a needle/plate-like morphology, and the peritectic η-Cu_6Sn_5 phase shows dendritic morphology in directionally solidified Sn-32at.% Cu peritectic alloy.

Figures 3(a) and (b) present the microstructures of the phase transition interface of the afore-mentioned Sn-32at.% Cu samples after deep etching, and the different phases are determined by the EDS analysis: 24.8at.% Sn [Point A in Fig. 3(d)], and 44.5at.% Sn [Point B in Fig. 3(d)]. The intermetallic compound η-Cu_6Sn_5, whose solubility is small, exhibits faceted feature with sharp edges. Further examination in Figs. 3(c) and (d) shows that an interesting round scallop sub-structure can be found in the magnified figures of Areas C and D in Figs. 3(a) and (b). These substructures are gradually surrounded by smooth facet planes during crystal growth, as

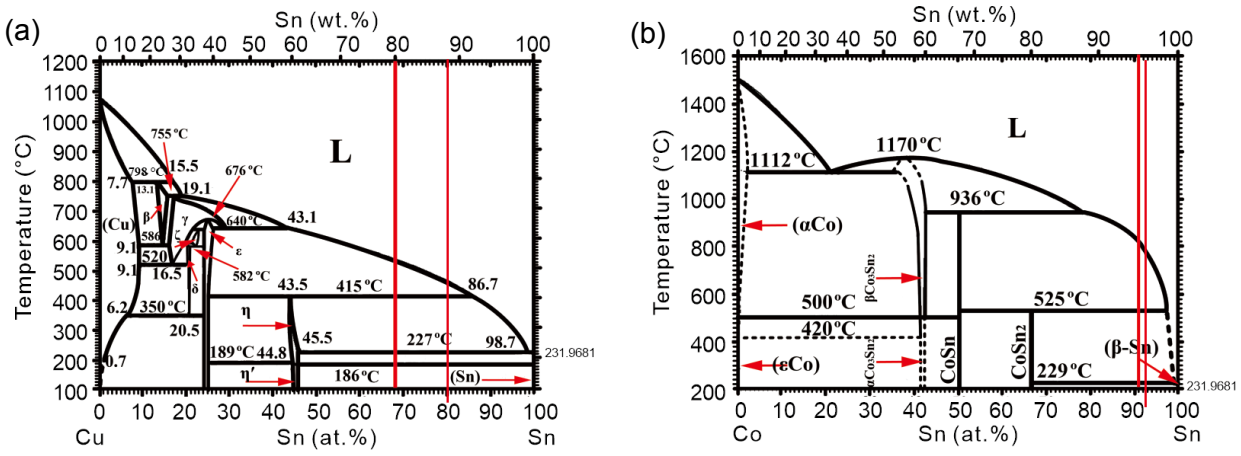

Fig. 1: Sn-Cu (a) and Sn-Co (b) binary alloy phase diagrams where the red vertical lines show the composition of Sn-32at.% Cu and Sn-9at.% Co peritectic alloys in this work, respectively [23, 31]

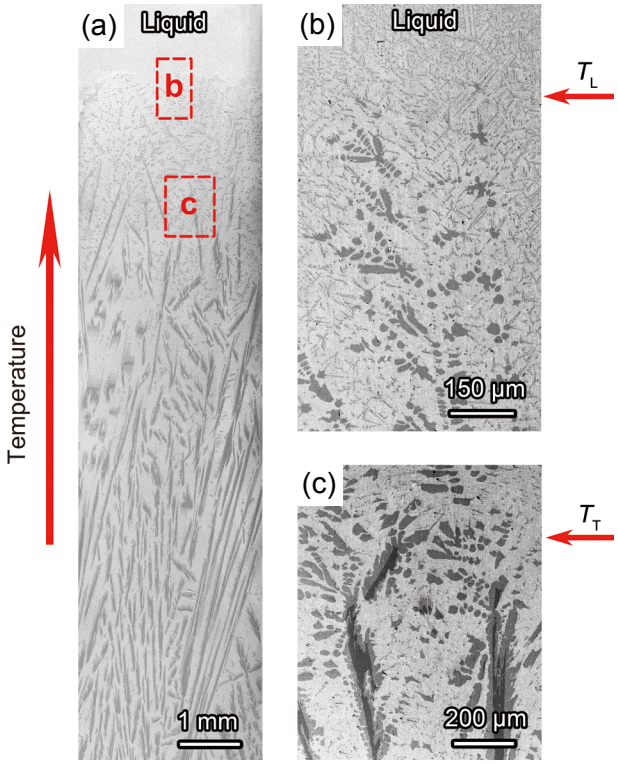

Fig. 2: Microstructures of directionally solidified Sn-32at.% Cu peritectic alloy before deep etching at growth velocity of 10 μm·s^{-1}: (a) longitudinal view; (b) solid/liquid interface at Area b in (a); (c) phase transition interface at Area c in (a)

presented in Figs. 3(e) and (f). Furthermore, after comparing the microstructures at different growth velocities in Figs. 3(c) and (d), it is found that the peritectic η-Cu_6Sn_5 phase becomes hexagonal at a higher growth velocity.

In addition to the peritectic Cu_6Sn_5 phase formed through peritectic reaction, Figs. 3(g) and (h) show the dendritic morphology of the peritectic Cu_6Sn_5 phase which grows directly from the melt. Similar to Figs. 3(c) to (f), the scallop-shaped sub-structure can be seen at both growth velocities; the faster the growth velocity, the more obvious the hexagonal characteristics of the peritectic Cu_6Sn_5 phase. Figures 4(a) to (c) exhibit the SEM images of the peritectic η phases at different positions of the sample at growth velocity of 10 μm·s^{-1}. It can be found that the peritectic Cu_6Sn_5 phases have different morphologies even at a constant growth velocity. At the positions of higher temperature of the sample, the peritectic Cu_6Sn_5 grains maintain a round scallop shape morphology. As the temperature decreases, the Cu_6Sn_5 grains become faceted with sharp edges and corners near the phase transition interface, and the grain size is obviously larger. In addition, as shown in Fig. 4, the long prismatic structure of Cu_6Sn_5 grains can be observed at lower temperature near the initial growth interface, and the center of these prismatic structures are empty.

Figure 5 exhibits the phase morphologies in the Sn-9at.% Co peritectic alloy at the growth velocity of 1 μm·s^{-1} before and after deep etching. The EDS results (65.6at.% Sn) show that the dendrites are composed of peritectic $CoSn_2$ phases. The

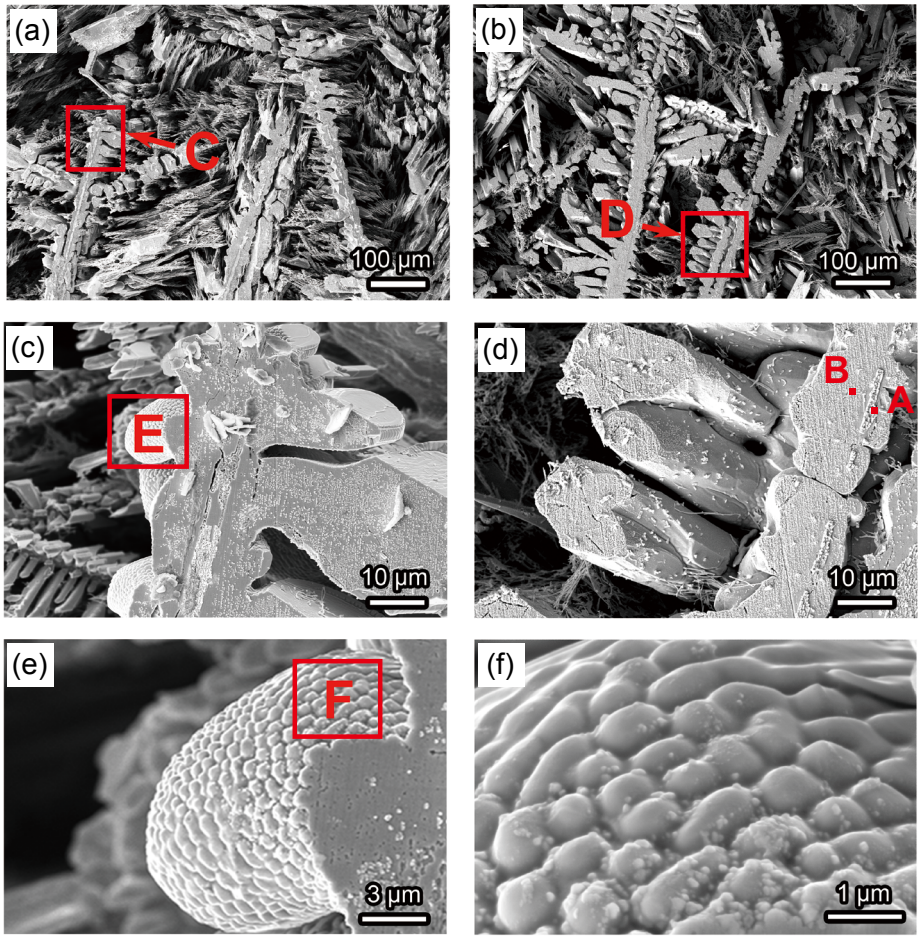

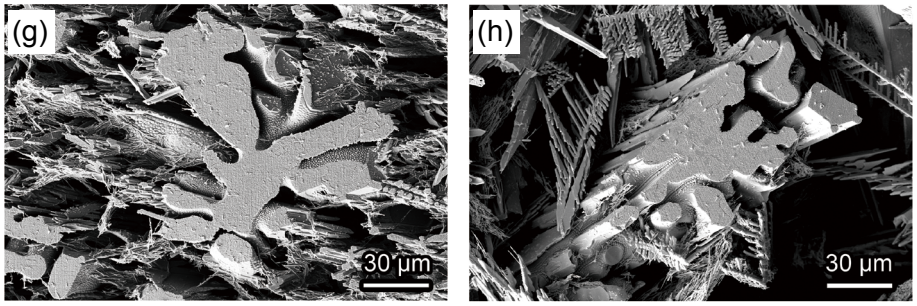

Fig. 3: Microstructures of directionally solidified Sn-32at.% Cu peritectic alloy after deep etching: the phase transition interface at growth velocities of 10 μm·s^{-1} (a) and 20 μm·s^{-1} (b); the sub-structures of the peritectic phases at growth velocities of 10 μm·s^{-1} (c) and 20 μm·s^{-1} (d); (e) partial enlarged view of (c); (f) partial enlarged view of (e); dendritic morphologies of peritectic phases at growth velocities of 10 μm·s^{-1} (g) and 20 μm·s^{-1} (h)

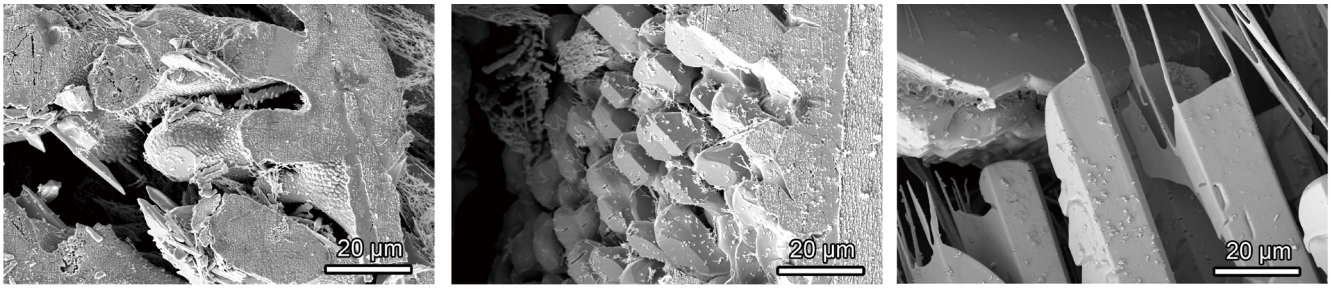

Fig. 4: Microstructures of peritectic η phases at different positions of directionally solidified Sn-32at.% Cu peritectic alloy at the growth velocity of 10 μm·s^{-1}

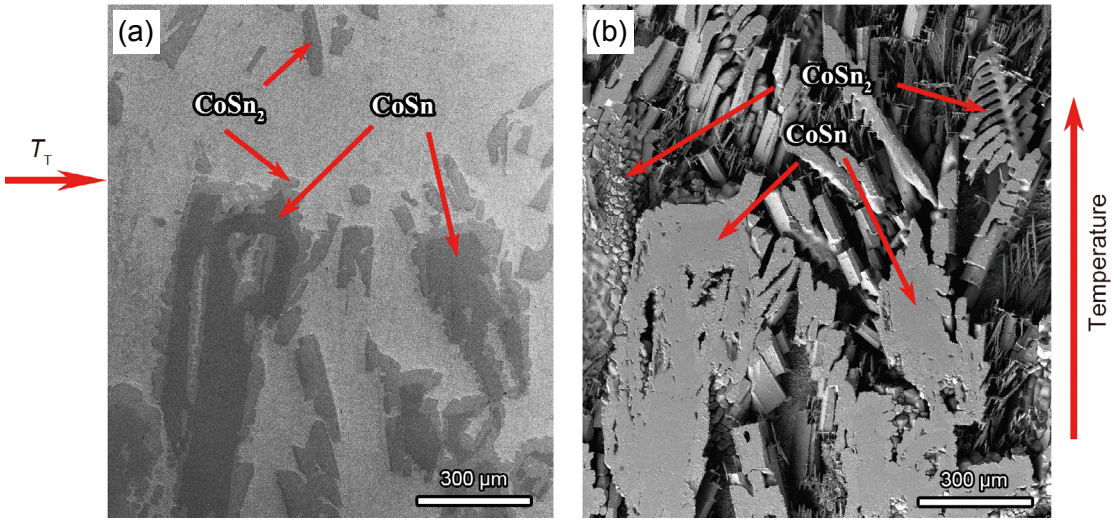

Fig. 5: Microstructures of the directionally solidified Sn-9at.% Co peritectic alloy at the growth velocity of 1 μm·s^{-1} before (a) and after (b) deep etching

sub-structure of primary CoSn phase cannot be observed even after deep etching. As can be seen in Fig. 5, the leading phase which first precipitates from the melt during directional solidification changes from primary CoSn phase to peritectic $CoSn_2$ phase when the temperature reaches the phase transition temperature (T_T). After etching, it can be observed that there are coarse peritectic $CoSn_2$ dendrites and bulk primary CoSn phases above and below T_T, respectively, which are consistent with those observed before etching. The primary CoSn phase shows a typical faceted morphology while the $CoSn_2$ phase has a dendritic morphology. It is interesting to find that the CoSn and $CoSn_2$ phases are both IMCs with nil solubility according to the equilibrium phase diagram, but their morphologies are quite different. Besides, after etching, it can be observed that the secondary arms of the $CoSn_2$ dendrites show quadrangular prism-like morphologies.

Similarly, Figs. 6(a) and (b) present the morphologies of the Sn-9at.% Co sample at the growth velocity of 5 μm·s^{-1} before and after deep etching, respectively, and the dendritic morphologies of peritectic $CoSn_2$ phase can also be clearly observed. Besides, the dendritic structures of peritectic $CoSn_2$ phases at the growth velocity of 5 μm·s^{-1} are finer and more

regular than that at 1 μm·s^{-1}. As shown in Fig. 7(a), it is interesting to find that the secondary dendrite arms of $CoSn_2$ phase show stepped morphologies although the peritectic $CoSn_2$ phase displays a typical dendritic morphology. After measuring in Fig. 6(b), it can be obtained that the angle between the growth direction of the primary dendrite and the secondary arm is nearly 45°. Simultaneously, the growth direction of most secondary arms is close to the temperature gradient direction.

In addition, as shown in Fig. 7(b), further examination on the roots of the secondary dendrite arms reveals the existence of flake-like microstructures which are perpendicular to the direction of the temperature gradient. These flake-like microstructures are surrounded by rod-like microstructures, and these sub-structures cannot be observed in the morphologies before etching. To determine the compositions of these sub-structures, EDS analysis was carried out, and the results show that the flake-like sub-structure and the rod-like sub-structure are $CoSn_4$ phases. $CoSn_4$ phase is a metastable phase, which cannot be formed in equilibrium solidification. Its formation in this sample is caused by quenching. Li et al. [30] proposed that the $CoSn_2$ grains tend to grow in the [001] direction and exhibit a quadrangular prism-like morphologies, while the $CoSn_4$ grains grow in a spiral manner and have a multi-layer structure.

4 Discussion

As discussed above, different growth types have been observed on the IMCs in both Sn-Cu and Sn-Co peritectic systems. The facted morphologies of the IMC Cu_3Sn phase which should present a non-faceted growth type in theory were found. Similarly, the non-facted dendritic morphologies of the IMC $CoSn_2$ phase which should present a faceted growth type in theory were also observed. To determine which phase is more likely to grow in a non-faceted way, Saroch et al. [40]

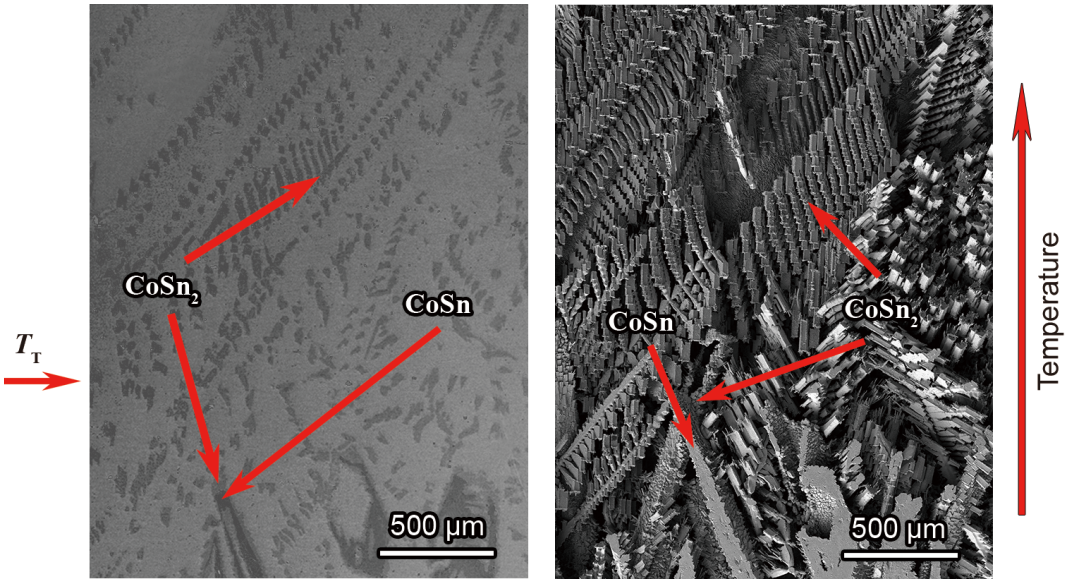

Fig. 6: Microstructures of the directionally solidified Sn-9at.% Co peritectic alloy at the growth velocity of 5 μm·s^{-1} before and after deep etching

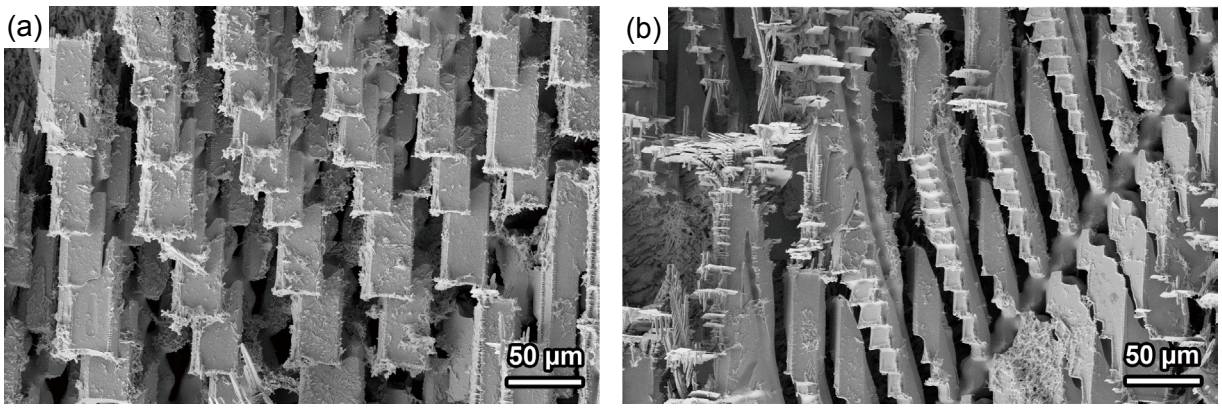

Fig. 7: Sub-structures of the secondary dendrite arms of $CoSn_2$ phase in directionally solidified Sn-9at.% Co peritectic alloy at the growth velocity of 5 μm·s^{-1} after deep etching: (a) the stepped microstructure; (b) the flake-like microstructure which are penetrated with the rod-like microstructures

proposed that the smaller the calculated values of ΔS^{ST} (entropy of solution) and $d\Delta S^{ST}/dT$ (the changing rate of entropy of solution with temperature), the more likely the non-faceted morphology occurs. $d\Delta S^{ST}/dT$ can be expressed as [40]:

$$\frac{d\Delta S^{ST}}{dT} = \frac{1}{m_S}\frac{\partial \Delta S^{SL}}{\partial x_e^S} + \frac{1}{m_L}\frac{\partial \Delta S^{SL}}{\partial x_e^S} \quad (1)$$

where m_S and m_L are the slopes of the solidus and liquidus lines, respectively. x_e^S is the solute (Sn) concentration in the solid phase, $\partial \Delta S^{SL}$ is the changing rate of entropy of solution with the solute concentration in the solid phase. In this work, the values of $\left(\partial \Delta S^{SL}\right)/\left(\partial x_e^S\right)$ of these two phases are assumed to be equal for simplicity. Then, the effect of $\left(\partial \Delta S^{SL}\right)/\left(\partial x_e^S\right)$ on $d\Delta S^{ST}/dT$ can be ignored. For the convenience of description, S_i was defined as:

$$S_i = \frac{1}{m_S} + \frac{1}{m_L} \quad (2)$$

Therefore, for a solid phase, the smaller S_i means the smaller value of $d\Delta S^{ST}/dT$, then the non-faceted morphology is more likely to occur. The values of m_S and m_L are usually obtained from the phase diagram [23, 26, 27]. Here, the Sn-Co peritectic alloy is taken as an example for analysis. As shown in Fig. 1(b), since both $CoSn_2$ and CoSn phases are IMCs with nil solubility, and their solidus lines are perpendicular to the horizontal axis, their inverse values of m_S are approximately equal to zero. Thus, $S_i \approx 1/m_L$. According to Fig. 1, the value of m_L of $CoSn_2$ phase is smaller than that of CoSn phase. For $CoSn_2$ phase, larger S_i also means larger value of $d\Delta S^{ST}/dT$. Therefore, it can be concluded that the dendrite growth of the $CoSn_2$ phase cannot be observed, which is contrary to the experimental results.

To resolve this discrepancy, the solubility of the IMCs should be re-examined. It should be noted that if the solubility of the IMC is not nil, the inverse values of m_S for these phases are not zero. According to Eq. (1), the difference in m_S between CoSn and $CoSn_2$ phases will influence the values of $d\Delta S^{ST}/dT$, which will lead to a different result. Then, to determine the solubility ranges of these IMCs, the compositions of both the CoSn and $CoSn_2$ phases in the Sn-9at.% Co samples at each growth velocity were identified with EDS.

Figure 8 shows the Sn concentrations in the CoSn and $CoSn_2$ phases at different growth velocities. Taking the sample at the growth velocity of 1 μm·s^{-1} for instance, the difference between the maximum and minimum Sn content in the CoSn phase is 0.55%. The difference between the maximum and minimum Sn content in the $CoSn_2$ phase is 0.74%. Thus, the solubility range of Sn content in the $CoSn_2$ phase is 34.5% larger than that in the CoSn phase. Similarly, for other samples, the solubility range of the $CoSn_2$ phase is also greater than that of the CoSn phase. This means that the $CoSn_2$ phase has a larger solubility than the CoSn phase.

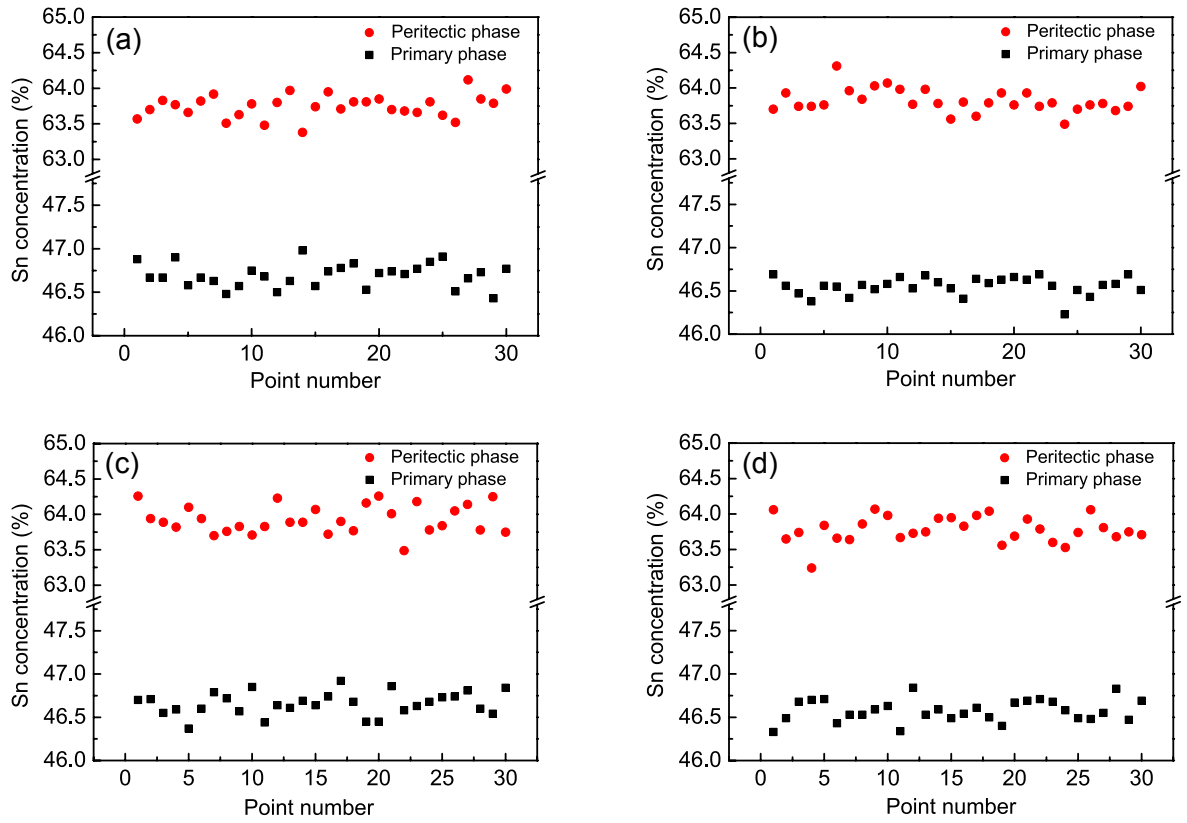

Fig. 8: Sn compositions in the primary and peritectic phases in Sn-9at.%Co peritectic alloys at different growth velocities: (a) v=1 μm·s^{-1}; (b) v=5 μm·s^{-1}; (c) v=10 μm·s^{-1}; (d) v=100 μm·s^{-1}

Although the exact values of m_S of these two phases cannot be obtained from the equilibrium phase diagram in Fig. 1(b), a rough calculation can still be performed by the solubility range (C_f):

$$m_S \approx \frac{2\left(T_p - T_r\right)}{C_f} \quad (3)$$

where T_p is peritectic reaction temperature which can be found in the equilibrium phase diagram, which are 936 °C and 525 °C for CoSn and $CoSn_2$ phases, respectively. T_r is the room temperature (T_r=25 °C). Integrating the data of these two phases at the growth velocity of 1 μm·s^{-1} into Eq. (3), the m_S values of CoSn and $CoSn_2$ phases can be obtained as −3,312.7 K·(at.%)$^{-1}$ and −1,351.4 K·(at.%)$^{-1}$, respectively. Then, the S_i values of CoSn and $CoSn_2$ phases are -1.05×10^{-2} (at.%)·K^{-1} and -1.07×10^{-2} (at.%)·K^{-1}, respectively. Obviously, the Si values of $CoSn_2$ phase are smaller, thus, the calculated values of ΔS^{ST} and $d\Delta S^{ST}/dT$ of $CoSn_2$ phase are smaller. Therefore, the dendritic morphology of the $CoSn_2$ phase can be observed. In addition, the dendritic growth of Cu_6Sn_5 phase in Fig. 1 can also be analyzed with the same method.

5 Conclusion

In this work, the growth morphologies of IMCs were analyzed during directional solidification of both the Sn-Cu and Sn-Co peritectic systems. The examination on solidified microstructure before acid corrosion shows that the dendritic growth of both the peritectic Cu_6Sn_5 and $CoSn_2$ phases can be observed in the Sn-Cu and Sn-Co alloys, respectively. However, the analysis on the dendritic morphologies of both the Cu_6Sn_5 and $CoSn_2$ phases after deep acid corrosion shows that these dendrites are composed of small sub-structures with faceted morphology. In addition, different growth types are observed on the IMCs in both Sn-Cu and Sn-Co peritectic systems. The facted morphologies of the Cu_3Sn and $CoSn_2$ IMCs are found in the experiment, which should present non-faceted growth type in theory. In order to clarify this phenomenon, the solubility ranges of these IMCs have been estimated, which confirms the dendritic morphology of the solidified phases whose solubility ranges are greater during peritectic solidification.

Acknowledgements

The authors would like to express gratitude for the support of the National Natural Science Foundation of China (Grant No. 51871118), the Fast Support Project (Grant No. JZX7Y20210162400301), and the fund of State Key Laboratory of Special Rare Metal Materials (Grant No. SKL2020K003).

References

[1] Peng P, Zhang A Q, Yue J M, et al. Investigation on morphology evolution of secondary branch during peritectic solidification in a temperature gradient through morphology characteristic: Experimental measurement and prediction. Mater. Chem. Phys., 2021, 256: 123674.
[2] Zou P F, Wang H P, Zheng C H, et al. Electrostatic levitation processing and microscopic hardness property of hyperperitectic Ti60Ni40 alloy. Intermetallics, 2021, 130: 106934.
[3] Feng L, Zhong J H, Zhu C S, et al. Multi-phase field simulation of multi-grain peritectic transition in multiple phase transformation. China Foundry, 2020, 17(5): 357–363.
[4] Lü P, Wang H P, Wei B, et al. Competitive nucleation and growth between the primary and peritectic phases of rapidly solidifying Ni-Zr hypoperitectic alloy. Metall. Mater. Trans. A, 2019, 50(2): 789.
[5] Biswas K, Hermann R, Wendrock H, et al. Effect of melt convection on the secondary dendritic arm spacing in peritectic Nd-Fe-B alloy. J. Alloys Compds., 2009, 480(2): 295–298.
[6] Arai Y, Emi T, Fredriksson H, et al. In-situ observed dynamics of peritectic solidification and δ/γ transformation of Fe-3 to 5 at. pct Ni alloys. Metall. Mater. Trans. A, 2005, 36(11): 3065–3074.
[7] Kerr H W, Kurz W. Solidification of peritectic alloys. Inter. Mater. Rev., 1996, 41(4): 129–164.
[8] Li C, Wu Y Y, Li H, et al. Morphological evolution and growth mechanism of primary Mg_2Si phase in Al-Mg_2Si alloys. Acta Mater., 2011, 59(3): 1058–1067.
[9] Su H J, Zhang J, Liu L, et al. Rapid growth and formation mechanism of ultrafine structural oxide eutectic ceramics by laser direct forming. Appl. Phys. Lett., 2011, 99(22): 1174.
[10] Çadırlı E, Böyük U, Kaya H, et al. The effect of growth rate on microstructure and microindentation hardness in the In-Bi-Sn ternary alloy at low melting point. J. Alloys Compds., 2009, 470(1–2): 150–156.
[11] Kang H J, Wang T M, Li X Z, et al. Faceted-nonfaceted growth transition and 3-D morphological evolution of primary Al_6Mn microcrystals in directionally solidified Al-3at.% Mn alloy. J. Mater. Res., 2014, 29(11): 1256–1263.
[12] Wang M N, Wang J Q, Feng H, et al. Effect of Ag_3Sn intermetallic compounds on corrosion of Sn-3.0Ag-0.5Cu solder under high-temperature and high-humidity condition. Corros. Sci., 2012, 63: 20–28.
[13] Dorin T, Stanford N, Birbilis N, et al. Influence of cooling rate on the microstructure and corrosion behavior of Al-Fe alloys. Corros. Sci., 2015, 100: 396–403.
[14] Kurz W, Fisher D J. Fundamentals of solidification. Trans. Tech. Publications Ltd., Switzerland, 1998.
[15] Dubost B, Lang J M, Tanaka M, et al. Large AlCuLi single quasicrystals with triacontahedral solidification morphology. Nature, 1986, 324(6092): 48–50.
[16] Abe E, Yan Y, Pennycook S J. Quasicrystals as cluster aggregates. Nat. Mater., 2004, 3: 759–767.
[17] Peng P, Li X Z, Liu D M, et al. Effect of peritectic reaction on dendrite coarsening in directionally solidified Sn-36at.% Ni alloy. J. Mater. Sci., 2012, 47(16): 6108–6117.
[18] Ma D, Li Y, Ng S C, et al. Unidirectional solidification of Zn-rich Zn-Cu peritectic alloys: II. Microstructural length scales. Acta Mater., 2000, 48(2): 419–431.
[19] Marsh S P, Glicksman M E. Overview of geometric effects on coarsening of mushy zones. Metall. Mater. Trans. A, 1996, 27(3): 557–567.
[20] Singh H, Gokhale A M, Tewari A, et al. Three-dimensional visualization and quantitative characterization of primary silicon particles in an Al-Si base alloy. Scripta Mater., 2009, 61(4): 441–444.
[21] Contieri R J, Rios C T, Zanotello M, et al. Growth and three-dimensional analaysis of Nb-Al-Ni ternary eutectic. Materials Characterization, 2008, 59(6): 693–699.
[22] Li B, Brody H D, Kazimirov A. Synchrotron microradiography of temperature gradient zone melting in directional solidification. Metall. Mater.Trans. A, 2006, 37(3): 1039–1044.

[23] Mehreen S U, Nogita K, McDonald S, et al. Suppression of Cu_3Sn in the Sn-10Cu peritectic alloy by the addition of Ni. J. Alloys Compds., 2018, 766: 1003–1013.
[24] He H, Huang S, Ye Y, et al. Microstructure and mechanical properties of Cu joints soldered with a Sn-based composite solder, reinforced by metal foam. J. Alloys Compds., 2020, 845: 156240.
[25] Li Z H, Tang Y, Guo Q W, et al. A diffusion model and growth kinetics of interfacial intermetallic compounds in Sn-0.3Ag-0.7Cu and Sn-0.3Ag-0.7Cu-0.5CeO_2 solder joints. J. Alloys Compds., 2019, 818: 152893.
[26] Zhai W, Wang W L, Geng D L, et al. A DSC analysis of thermodynamic properties and solidification characteristics for binary Cu-Sn alloys. Acta Mater., 2012, 60: 6518–6527.
[27] Lü H, Li S, Liu L, et al. Peritectic phase growth in directionally solidified Cu-70% Sn alloy. Sci. China Phys. Mech. Astron., 2007, 50(4): 451–459.
[28] Zhai W, Wei B. Direct nucleation and growth of peritectic phase induced by substantial undercooling condition. Mater. Lett., 2013, 108: 145–148.
[29] Zhai W, Hong Z Y, Wen X L, et al. Microstructural characteristics and mechanical properties of peritectic Cu-Sn alloy solidified within ultrasonic field. Mater. Des., 2015, 72: 43–50.
[30] Li L, Suo Y S, Ban C Y, et al. Growth behaviors of $CoSn_2$/$CoSn_4$ composite particles in the solidification of Sn-Co alloy under a high magnetic field. J. Alloy Compds., 2020, 816: 152540.
[31] Wang C, Kuo C, Huang S, et al. Temperature effects on liquid-state Sn/Co interfacial reactions. Intermetallics, 2013, 32: 57–63.
[32] Yakymovych A, Shtablavyi I, Mudry S. Structural studies of liquid Co-Sn alloys. J. Alloys Compds., 2014, 610(1): 438–442.
[33] Liu J M, Zhai W, Wang B J, et al. Structure and property modulation of primary CoSn and peritectic $CoSn_2$ intermetallic compounds through ultrasonicating liquid Sn-10%Co alloy. J. Alloys Compds., 2010, 827: 154297.
[34] Wang S H, Yi Z, Wang X X, et al. A rational design to buffer volume expansion of CoSn intermetallic in lithium and sodium storage: Multicore-shell versus monocore-shell. Energy Storage Mater., 2019, 23: 629–635.
[35] González J R, Alcántara R, Nacimiento F, et al. CoSn-graphite electrode material prepared by using the polyol method and high-intensity ultrasonication. Electrochim. Acta, 2011, 56(27): 9808–9817.
[36] Wang C H, Chen S W. Cruciform pattern formation in Sn/Co couples. J. Mater. Res., 2007, 22(12): 3404–3409.
[37] Wang C H, Kuo C Y, Huang S E, et al. Temperature effects on liquid-state Sn/Co interfacial reactions. Intermetallics, 2013, 32: 57–63.
[38] Chen S W, Chen Y K, Wu H J, et al. Co solubility in Sn and interfacial reactions in Sn-Co/Ni couples. J. Electron. Mater., 2010, 39(11): 2418–2428.
[39] Peng P, Yang J R, Li X Z, et al. Composition-dependent phase substitution in directionally solidified Sn-22at.% Ni peritectic alloy. J. Mater. Sci., 2016, 51(3): 1512–1521.
[40] Saroch M, Dubey K S, Ramachandrarao P. On the composition dependence of faceting behaviour of primary phases during solidification. J. Cryst. Growth, 1993, 126(4): 701–706.